Mechanics of Advanced Composite Structures

Journal homepage: https://macs.semnan.ac.ir/

Semnan University

ISSN: 2423-7043

Research Article

Experimental and Numerical Investigation on Buckling Load Prediction of Sandwich Cylinders with Hyperelastic Cores Using the Vibration Correlation Technique

Mojtaba Rahmani Gheshlaghi, Gholamhossein Rahimi *

Department of Mechanical Engineering, Tarbiat Modares University, Tehran, Iran

A R T I C L E   I N F O

Article history:

Received: 2025-11-19

Revised:

Accepted:

Keywords:

Hyperelastic Core; Buckling Load; Vibration Correlation Technique (VCT);

Numerical Analysis;

Sandwich Shell;

A B S T R A C T

Considering the unique characteristics of sandwich structures in the optimal design of lightweight and high-strength components, their application in advanced engineering systems has been steadily increasing. These structures exhibit superior performance, particularly under buckling loads, unwanted vibrations, and energy absorption conditions. In this study, two cylindrical sandwich specimens were fabricated, consisting of a thermoplastic polyurethane (TPU) hyperelastic core and composite face sheets. The main objective of the experiments was to evaluate the accuracy of predicting the critical buckling load using the Vibration Correlation Technique (VCT). One specimen was subjected to a destructive test, while the other underwent a non-destructive test. The VCT, as a non-destructive and cost-effective approach, estimates the critical load by monitoring the variations in the natural frequencies of the specimen under axial compression up to the onset of instability. Modal analyses were performed using the impact test method, and the effects of parameters such as core thickness and fiber orientation of the composite faces were investigated. In addition, a three-dimensional numerical model was developed in ABAQUS to analyze the structural behavior under different loading conditions. A comparison between experimental and numerical results showed a minor discrepancy (approximately 3.6%) in the predicted buckling load. The findings indicate that the VCT is a reliable and accurate tool for estimating the buckling load in modern sandwich structures with hyperelastic cores.

1. Introduction

Buckling refers to the loss of structural stability, which can lead to significant financial losses or even catastrophic failures. Among various materials used in engineering structures, hyperelastic materials have attracted great attention due to their unique features such as high energy absorption capacity and resilience, making them widely applicable in modern industries. Meanwhile, the combination of composite face sheets with sandwich cores significantly enhances load-bearing capability, impact resistance, and overall structural performance. Such material systems are of special interest in the design of mechanical components where vibration control and energy dissipation are critical. Cylindrical shell structures made of composites play a vital role in numerous engineering applications due to their high load-carrying capacity and excellent stiffness-to-weight ratio. Recently, there has been a growing research interest in hyperelastic cylindrical shells, mainly because of their diverse industrial applications. A considerable number of studies have been carried out to predict the

* **Corresponding author.**
E-mail address: rahimi_gh@modares.ac.ir

Cite this article as:

Rahmani, M., Rahimi, Gh. And Hosseini, SH., 2026. Experimental and Numerical Investigation on Buckling Load Prediction of Sandwich Cylinders with Hyperelastic Cores Using the Vibration Correlation Technique. *Mechanics of Advanced Composite Structures*, 13(1), pp. xxx-xxx.

https://doi.org/10.22075/MACS.2025.39315.2050

buckling load and vibration behavior of sandwich and hyperelastic cylindrical structures. Arbelo et al. [1] investigated the advantages and limitations of the Vibration Correlation Technique (VCT) in predicting the buckling load of flat plates and cylindrical shells. Kalnins et al. [2] presented experimental data validating the high accuracy of VCT in estimating the buckling load of unreinforced cylindrical shells under axial compression. Abramovich et al. [3] applied the VCT as a non-destructive tool for evaluating the buckling load of thin-walled structures, examining reinforced aluminum cans and composite-stiffened columns. In a related study, Pagani et al. [4] proposed a one-dimensional finite element model based on the Carrera Unified Formulation (CUF) for analyzing hyperelastic soft materials and structures. Their model incorporated both geometric and material nonlinearities and utilized several strain energy functions such as neo-Hookean, Gent, and Fung–Demiray, which separate the strain energy into volumetric and isochoric parts to simulate near-incompressibility. Analytical expressions for the internal force vector and tangent stiffness matrix were derived, and validation against numerical examples such as uniaxial tension, bending, and thick-shell compression confirmed the model's high accuracy and computational efficiency. Aranda-Iglesias et al. [5] used a generalized membrane theory to model large-amplitude free vibrations of incompressible hyperelastic cylindrical shells. Zhang et al. [6] studied the linear vibration of thin cylindrical shells made of classical Mooney–Rivlin material. Wagner et al. [7] applied a multi-objective optimization method to determine the optimal stacking sequence of composite cylindrical shells under axial compression, considering geometric imperfections and fiber orientation. Similarly, Pitton et al. [8] proposed an optimization strategy for variable-stiffness cylindrical shells in aerospace applications, showing that curved fibers could increase the critical buckling load by about 4%. Franzoni et al. [9] experimentally validated the reliability of the VCT in estimating the buckling load of unreinforced composite cylindrical shells and extended its application to orthotropic shells under internal pressure. Mohammadzadeh et al. [10] designed and constructed an advanced four-axis filament winding system for manufacturing complex composite structures such as cylindrical, conical, and lattice geometries. The system enabled precise fiber placement through integration with 3D modeling software and resulted in specimens with improved fiber volume fraction and reduced voids, achieving a remarkable 24,000 N/kg buckling load-to-weight ratio in lattice configurations. Höller et al. [11] developed a new membrane theory for analyzing large deformations in graphene circular plates under axial loading, employing a hyperelastic density functional theory (DFT) framework. Xu et al. [12] investigated temperature-dependent nonlinear responses of moderately thick hyperelastic cylindrical shells using third-order shear deformation theory and the Arruda–Boyce model. Khaniki et al. [13] analyzed geometric imperfections in hyperelastic beams using the dynamic equilibrium method, revealing their influence on longitudinal and transverse displacements. Aurilia et al. [14] examined the influence of organo-modified layered silicates (OMLS) on the microstructure and dynamic properties of TPU, finding improvements in viscoelastic behavior and stiffness. Mehta et al. [15] studied the deformation of thick flexible cylindrical conduits under internal pressure. Saeidiha et al. [16] analyzed the fundamental resonance characteristics of thin hyperelastic cylindrical shells subjected to external loads. Duc et al. [17] optimized the fiber angles of multilayered composite shells to maximize natural frequencies, while Coskun et al. [18] developed a multi-step optimization framework that achieved a 41% increase in buckling load for variable-stiffness shells. Zhang et al. [19] investigated the effects of geometric imperfections on the resonant response of hyperelastic cylindrical shells, showing strong coupling between excitation, imperfection amplitude, and vibration behavior. Pagani et al. [20] recently proposed an integrated displacement-based formulation for analyzing large strains in compressible and nearly incompressible hyperelastic materials using the Carrera Unified Formulation. Choudhary [21] introduced an innovative hybrid approach combining analytical, finite element, and genetic algorithm methods for optimizing composite shells under combined axial and lateral pressures. Xin et al. [22] developed a deep learning-based technique for predicting buckling modes in composite cylindrical shells. Arani et al. [23] analyzed hyperelastic cylindrical shells with initial imperfections. Rezayat et al. [24] experimentally studied the mechanical behavior of advanced sandwich panels under quasi-static indentation loading, showing that incorporating an elastomeric interlayer between composite faces and aluminum honeycomb cores enhanced strength and energy absorption by 20%. Liang et al. [25] modeled the nonlinear buckling characteristics of functionally graded concrete–steel cylindrical structures using artificial neural networks (ANNs). Sobotka et al. [26] proposed a nonlinear anisotropic elastic model for ePTFE vascular grafts, accurately predicting mechanical responses under tensile and inflation tests.

Finally, Liu et al. [27] developed a physics-informed deep learning framework for predicting buckling behavior of cylindrical shells under axial compression. Among these efforts, the Vibration Correlation Technique (VCT) remains a key and versatile method for estimating buckling loads through the analysis of natural frequency variations under mechanical loading. This approach, validated across numerous studies, is particularly valuable in industrial applications such as hydraulic pipeline systems, where excessive vibration and resonance-induced fatigue are common causes of structural failure.

Fig. 1. Vibration-induced failures in hydraulic pipelines [28].

Resonance occurs when the frequencies of fluid oscillations or base excitations approach the natural frequencies of the pipeline, leading to structural resonance. This phenomenon can cause significant relative displacements at the joints connecting the pipeline to fixed components. Figure 1 illustrates common examples of vibration-induced failures in hydraulic piping systems used in aircraft and other industrial applications. The use of soft materials such as rubber or vibration absorbers, as shown in Figure 2, is among the typical damping techniques employed to mitigate such vibrations. Since enhancing the damping coefficient is one of the inherent characteristics of hyperelastic materials, these materials are utilized in the present study to improve the overall vibration damping performance.

Fig. 2. Examples of proposed vibration energy dissipation devices [28, 29].

Baciu et al. [30] presented one of the most comprehensive recent studies, applying VCT to cylindrical shells subjected to combined axial and additional small perturbation loads. Their numerical and experimental results confirmed that VCT retains high prediction accuracy even under multiaxial loading scenarios, highlighting the method's robustness for practical engineering applications.

Likewise, Gliszczyński [31] expanded the applicability of the technique to unstiffened CFRP shells. This study provided an in-depth analysis of VCT sensitivity to geometric imperfections and model uncertainties, establishing a methodological foundation for evaluating composite structures with high imperfection sensitivity. In another important 2025 contribution, Yılmaz [32] applied VCT to steel plates under rotational restraints, demonstrating that the technique remains effective even for elements with non-standard or partially restrained boundary conditions. These findings collectively highlight the adaptability of VCT across a range of structural forms. In addition to shell and plate applications, recent research has begun to address the complexities of sandwich structures and hybrid systems. Rahmani Gheshlaghi et al. [33] introduced a hybrid computational–experimental framework for predicting buckling behavior in sandwich cylinders, incorporating VCT as part of an integrated validation strategy. Their results provide compelling evidence that VCT can be successfully combined with advanced numerical models—especially for systems where nonlinear material behavior must be captured accurately.

The Vibration Correlation Technique (VCT) has consistently demonstrated its effectiveness in estimating buckling loads in various types of structures, including shells, particularly with recent advances in geometric design and configuration optimization. Nevertheless, significant research gaps still exist regarding the application of the VCT for predicting the buckling load of cylindrical shells with hyperelastic cores and composite face sheets. The present study aims to address this gap by focusing on this unique class of sandwich cylindrical structures.

Comparing VCT with these commonly used approaches:

Acoustic methods (e.g., acoustic emission monitoring) are effective for detecting damage initiation and crack propagation but are less suited for predicting buckling loads, since they typically provide event-based signals rather than continuous stiffness-related information. In contrast, VCT provides a direct, continuous correlation between natural frequency evolution and pre-buckling stiffness, enabling earlier and more quantitative prediction of the critical load.

Digital Image Correlation (DIC) offers full-field deformation measurement and can capture the onset of mode-shape changes leading to buckling. However, DIC systems require high-resolution cameras, careful calibration, controlled lighting, and relatively complex data processing. In comparison, VCT is simpler, less equipment-intensive, and more cost-effective, while still providing accurate predictions. This comparison clarifies the strengths and limitations of VCT relative to other measurement techniques and reinforces its advantages for the class of structures investigated.

Unlike earlier VCT studies, which have focused primarily on metallic shells or sandwich structures with linear elastic cores, the current work is the first to experimentally and numerically evaluate VCT for sandwich cylinders incorporating a hyperelastic TPU core. Hyperelastic cores exhibit large-deformation, nonlinear mechanical behavior that fundamentally alters stiffness evolution during pre-buckling loading—conditions under which the VCT has not previously been validated.

Furthermore, this study introduces:

1. A combined destructive and non-destructive experimental program to assess VCT accuracy on identical specimens,

2. A detailed 3D finite-element model in ABAQUS that captures hyperelastic material behavior and validates the VCT predictions, and

3. An evaluation of the influence of core thickness and composite face-sheet fiber orientation on frequency–load relationships, which has not been addressed in prior VCT literature. These contributions demonstrate that VCT remains reliable even for structures with nonlinear hyperelastic cores, thereby extending its applicability to a broader class of modern lightweight sandwich components. The primary objective of this research is to estimate the critical buckling load of sandwich cylindrical shells composed of a hyperelastic core and composite face sheets using the VCT approach. In the first stage, a sandwich cylindrical specimen was fabricated, utilizing 3D printing for the flexible core and the filament winding technique for the inner and outer composite layers. Subsequently, using ABAQUS software, a parametric study was conducted to determine the optimal design parameters, including the core thickness and fiber orientation angle of the composite layers. This process allowed for the selection of a configuration that maximized both the buckling load-to-weight and natural frequency-to-weight ratios. Finally, the critical buckling load predicted by the VCT was compared with the corresponding experimental results for validation.

2. Geometrical Specifications and Fabrication of Experimental Specimens

In this study, a cylindrical shell was investigated, as illustrated in Figure 3. Certain geometrical parameters of the model were considered fixed, while others were treated as variables to identify their optimal values. The height and radius of the cylinder were taken as constant parameters, whereas the glass fiber orientation angle and core thickness were defined as variable parameters. The optimization of these parameters was carried out with respect to an objective function that aimed to maximize both the natural frequency and the buckling load. This optimization process was conducted through numerical simulations in ABAQUS prior to specimen fabrication, enabling the identification of optimal parameters for the manufacturing stage.

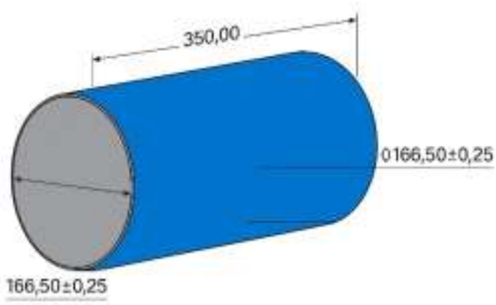

Fig. 3. The cylinder modeled in ABAQUS software

In this study, a cylindrical shell with hyperelastic cores and composite face sheets is designed such that two key performance indices, the ratio of the critical buckling load to the weight $\frac{p_0}{w} = p_{cr}$ and the ratio of the first critical natural frequency to the weight $((\frac{f_0}{w} = f_{cr})$ are optimized. To achieve this objective, several geometric parameters have been adjusted. As shown in Figure4, these parameters include the fiber orientations in the eight composite layers (θ_1 to θ_8) relative to the horizontal axis, the core thickness (t), the thickness of each layer (h), the inner diameter of the cylinder (R=155 mm), and the overall cylinder length (L=300 mm).

In this configuration, the fiber orientation angle alternates between even and odd layers, such that even layers are arranged at an angle of +α and odd layers at an angle of −α, as illustrated in Figure 4.

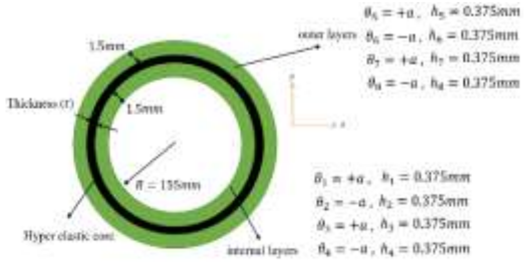

Fig. 4. Geometric parameters of the fabricated cylindrical specimen

Considering the specified conditions for fabricating the cylindrical shell with a hyperelastic core and composite face sheets, the core and composite layers are manufactured separately.

2.1. Fabrication of the Hyperelastic Core

The hyperelastic core was fabricated using 3D printing technology, as illustrated in Figure 5. The 3D printing parameters used for the specimens are presented in Table 1.

Table 1. 3D printing setup parameters

Specimens code	Nozzle speed (mm/s)	Nozzle Temp. (Deg. Cel.)	Plate Temp. (Deg. Cel.)	Wall Thk. (mm)	Nozzle Dia. (mm)	Thk. layer (mm)
Thermoplastic polyurethane	30	210	40	0.66	0.4	0.2

The above parameters were determined based on the data sheets provided by the material manufacturer and experimental experience. It is worth noting that the standard tensile test specimens were fabricated using the same 3D printing parameters as those of the actual samples, to ensure identical final mechanical properties, as shown in Figure 5. The hyperelastic core was printed upright along the cylinder axis. This orientation was selected to ensure uniform deposition around the circumference, minimize ovalization, and provide consistent layer bonding in the axial direction. The above parameters were determined based on the material manufacturer's datasheets and experimental experience. It is worth noting that standard tensile test specimens were fabricated using the same 3D printing parameters as the actual samples to ensure identical final mechanical properties, as shown in Figure 6.

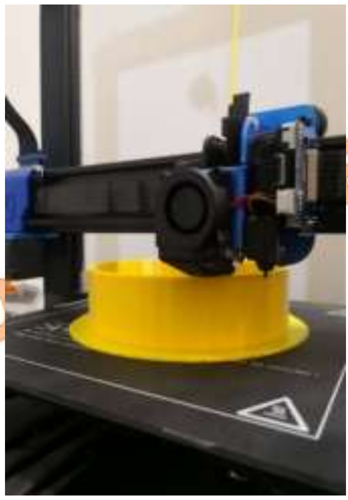

Fig. 5. 3D printing process of the main specimens

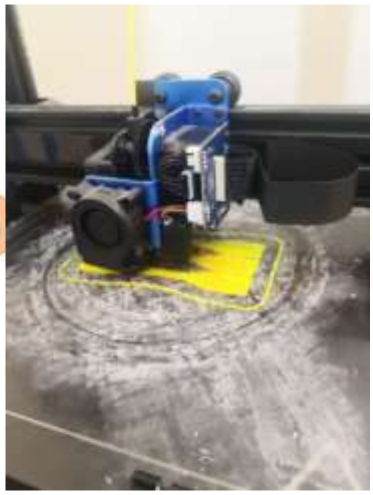

Fig. 6. 3D-printed standard specimens for tensile testing

2.2. Fabrication of the Composite Face Sheets

The composite layers of the specimens were fabricated using a CNC filament-winding machine, as illustrated in Figure 7. In this step, the machine's mold was stabilized using a chromed cylindrical mandrel to facilitate the filament winding process. Prior to production, a thin layer of polyvinyl wax was applied on the mold surface as a release agent to allow easy separation of the mold from the specimens. The fabrication process began by placing the mold onto the machine's mandrel, which is capable of rotational movement and adjustable horizontal translation. Both the rotational and horizontal speeds were carefully controlled within a specified range of manufacturing parameters to ensure that the grooves were properly filled with resin-impregnated fibers.

The key parameters in the fabrication process were as follows:

A) Glass Fiber tension: 1597 g
B) Rotational speed: 12 rpm
C) Epoxy Resin temperature: 25 °C

Other parameters were automatically calculated by the CNC machine. The resin-impregnated glass fibers were helically wound onto the rotating mandrel using a computer-controlled CNC filament winding machine. The winding angle was precisely maintained at ±30° for all eight layers (inner and outer face sheets). Each layer was wound continuously, and the fiber bands were placed adjacent to each other without gaps, forming a smooth, uniform cylindrical laminate. No intentional ribs or grooves were created; the final composite face sheets are smooth and consistent with the specimens tested experimentally. A specialized fiber feeding system was employed to accurately direct the fibers into the grooves. After the grooves were fully filled, a fabric layer was placed over the ribs and impregnated with resin. This procedure was repeated for the desired number of layers. After winding the inner cylinder on the mandrel, it was covered with the 3D-printed hyperelastic core, which acted as a new mandrel and a base for the outer composite face sheet. Both the inner and outer composite face sheets consisted of eight layers arranged at ±30° fiber orientations. These parameters are illustrated in Figure 4, and their extraction as the optimized structure from ABAQUS will be presented in the Results section.

Fig. 7. Fiber winding process

In the next step, after the fabrication process was completed, the specimens were cut and transferred to an autoclave for the curing process (as shown in Figure 8), which lasted a total of 12 hours: eight hours at 80 °C, followed by four hours at 120 °C.

Fig. 8. Final curing process of the specimens

After the fabrication of the test specimens and to prepare the areas for applying compressive loads in subsequent experiments, the two ends of the fabricated cylinders must be fully constrained; in other words, rotations and displacements at both ends should ideally be zero (except in the axial direction), which will be discussed later. This condition is particularly applied in the analytical study. As shown in Figure 9, the top and bottom edges of the shell are reinforced using a tab whose stiffness is greater than that of the structure. Initially, a mold capable of holding the cylinder dimensions is printed, and both ends are secured by adding resin into these molds.

Fig. 9. End tabs of the specimens

3. Experimental Tests for Determining Mechanical Properties

In this study, the objective was to minimize the maximum discrepancy between the experimental results and the numerical outputs. To achieve this goal, three standard TPU specimens were printed using the 3D printing parameters reported in Table 1 and in accordance with ASTM D638. The standard specimens were subjected to tensile testing to determine their mechanical properties, including the Young's modulus. It should be noted that for hyperelastic materials, obtaining the Young's modulus through these tests allows for the extraction of appropriate values for related coefficients, depending on the chosen material functions and the relationships between these coefficients and the Young's modulus.

To determine the properties of the composite specimens for numerical simulations and analytical applications, the NOL (Naval Ordnance Laboratory) method was employed in accordance with ASTM D 2290-04. The complete orthotropic elastic constants of the composite face sheets were determined using different ASTM standards:

- **E_1 (longitudinal modulus) and ν_{12} (major Poisson's ratio):** ASTM D3039 – tensile test on [0°] laminates.

- **E_2 (transverse modulus):** ASTM D2290-04 (NOL ring test) – hoop tensile test of filament-wound rings; this method directly provides the transverse stiffness of a cylindrical shell.
- **G_{12} (in-plane shear modulus):** ASTM D3518 – tensile test on [±45°] laminates. All composite test specimens were fabricated with the same filament winding parameters and cured under identical conditions as the main cylindrical shells.

The advantages of this method include its non-destructive nature, cost-effectiveness in specimen preparation and testing, and high accuracy of the results. The obtained results will be discussed in the Results section.

Fig. 10. Tensile testing of the standard specimens

4. Modal Testing of the Fabricated Specimens

Modal analysis and impact hammer tests were conducted under variable axial compressive loads to investigate how the first-mode vibration frequency changes at different compressive load levels below the critical buckling load, which is approximately obtained from numerical methods such as ABAQUS (Figure 11). During the operation, the machine jaws move slowly to ensure loading occurs within the static range at a low strain rate. Once the desired compressive load is reached, the loading is stopped. The specimens are then subjected to accelerometer and load cell measurements, with hammer impacts applied at each step. This produces force-time and acceleration-time data. A crucial aspect of this process is ensuring data reliability by repeating each test three times. This means that at each loading step, the hammer strikes the structure three times, and the outputs for each stage are recorded for each specimen. An important consideration in this step is timing: due to potential hydraulic pressure drops in the testing machine, prolonging the repetition of these three tests could lead to pressure variations between the first and last trials, introducing minor errors. Therefore, minimizing the elapsed time during this step while maintaining accuracy helps ensure consistency of results and naturally reduces error. Finally, MODALVIEW software was used to perform a Fast Fourier Transform (FFT) and analyze the Frequency Response Functions (FRF) to extract modal parameters, including natural frequencies and mode shapes. The resulting data were recorded for subsequent use in VCT calculations.

Fig. 11. Modal test setup of the experimental specimens

5. Steps for Implementing the Vibration Correlation Technique (VCT)

Initial condition, geometry, and material imperfections are among the primary reasons for employing the VCT method. To account for this important factor) especially due to the use of cylindrical geometry and hyperelastic materials, VCT is applied, and the knockdown factor is calculated. Using this technique, ideal results are brought closer to reality, and as shown in Table 9, applying VCT and the knockdown factor significantly improves agreement with experimental results. This demonstrates the method's effectiveness in accounting for imperfections and modifications that reduce the buckling load, yielding more accurate and reliable predictions. The following steps are followed to predict the critical buckling load of sandwich cylindrical shells with hyperelastic cores and composite layers using VCT:

Step 1: Calculate the critical buckling load (P_0) for the sandwich cylindrical shells with hyperelastic cores and composite layers. This can be done using a finite element model or an analytical approach.

Step 2: Determine the natural frequency (f_0) of the sandwich cylindrical shells under zero applied load. Similar to Step 1, this can be obtained using a finite element model or an analytical method.

Step 3: Begin measuring the natural frequencies of the loaded structure. As the load is gradually increased, track the changes in natural frequency up to 70% of the buckling load identified in Step 1. The knockdown factor (ξ^2), representing the ratio of the buckling load of an imperfect shell to that of a perfect cylindrical shell, is then calculated using the squared natural frequencies plotted against the applied load. The initial method for calculating the knockdown factor was introduced by Souza [34], involving a linear fit between $(1-P)^2$ and $(1-f^2)$, where $P=\frac{P_l}{P_0}$ and $f=\frac{f_l}{f_0}$. Here, P_l is the applied load at each step, P_0 is the axial critical buckling load, f_0 is the first-mode frequency under zero load, and f_l is the measured frequency at the given load. However, as noted by Arbelo et al. [1], when this method is applied to sandwich cylindrical shells with hyperelastic cores and composite layers, it can produce negative knockdown factors (ξ^2), which are physically meaningless. Consequently, they [1, 35] proposed an alternative approach: instead of a linear fit, a second-order curve fit is used, and the knockdown factor is defined as the minimum value of $(1-P)^2$. In this study, the knockdown factor is extracted using the method developed by Arbelo et al. [1]. The necessary data for implementing VCT at this stage can be obtained from FEM simulations or experimental tests.

Step 4: Finally, the critical buckling load can be estimated using the following equation [1, 36]:

$$P_{VCT}=P_{cr}\left(1-\sqrt{\xi^2}\right) \tag{1}$$

The knockdown factor (ξ^2) is obtained using the second-order curve fit of $(1-P)^2$ versus $1-f^2$. We now provide a physical justification for the use of a second-order fit in the VCT implementation.

The key reason is that sandwich cylindrical shells with a hyperelastic core exhibit both geometric and material nonlinearities even at relatively small fractions of the critical load. The bending–stretching coupling in the composite face sheets, combined with the nonlinear stress–strain behavior of the hyperelastic core, introduces a mildly nonlinear stiffness reduction as load increases. This stiffness degradation does not follow a purely linear trend with respect to load, which is consistent with observations from our FE simulations as well as the experimental frequency–load data.

As a result, the relationship between the nondimensional load parameter (1 – P/Pcr) and the nondimensional frequency parameter ($1-f^2/f_0{}^2$) deviates from strict linearity. The curvature of this relationship is small but systematic, and the second-order polynomial provides the minimal order necessary to capture this nonlinear behavior without overfitting. Importantly:

the first-order term reflects the linear stiffness reduction typical of thin shells, while the second-order term captures the additional softening effect introduced by the hyperelastic core's nonlinear response as deformation progresses. Therefore, the second-order fit is not chosen arbitrarily; it reflects the physical response of the sandwich structure where core compressibility, shear deformation, and strain-dependent stiffness contribute to a slightly curved frequency–load correlation. From a physical perspective, the curved frequency-load relationship in hyperelastic-cored sandwich cylinders arises from three interacting mechanisms: (i) the progressive stiffening of the composite face sheets due to in-plane membrane stresses, (ii) the nonlinear shear deformation of the TPU core which exhibits strain-dependent stiffness, and (iii) the moderate compressibility of the core ($\nu = 0.39$) that leads to a small but measurable volumetric deformation under axial compression. Unlike metallic shells where the frequency drop is almost purely geometric, here the material nonlinearity contributes approximately 12–15% of the total frequency reduction at 70% of Pcr, as quantified by comparing a linear elastic core simulation (not shown for brevity) with the present hyperelastic model. This validates that a purely linear fit would underestimate the knockdown factor, and a second-order polynomial is the minimal physically consistent representation.

6. Damping Ratio

One of the advantages of using a hyperelastic core is the improvement of the damping ratio. Therefore, the hyperelastic core employed in the cylindrical shell structure also increases the energy dissipation capacity. Several methods exist to calculate the damping ratio, with the impact hammer test being one of the most accurate. Since this test was already performed for VCT application, the results can also be used to calculate the damping ratio. The output curves are analyzed accordingly [37]. Based on previous studies, the relationship between the damping ratio and the natural frequencies obtained from the hammer test is reported in the next stage.

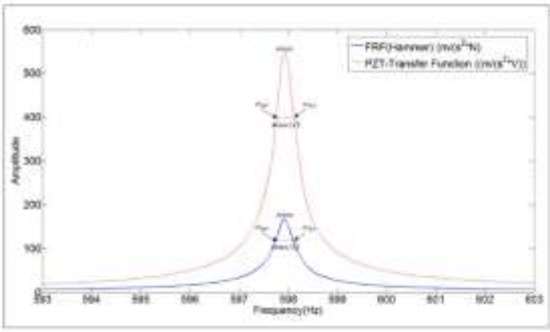

Fig. 12. Method for calculating the damping ratio [37]

It is worth noting that the damping ratio of the sandwich cylinder is not solely determined by the hyperelastic core; the composite face sheets also contribute through interlaminar friction and viscoelastic dissipation of the epoxy matrix. However, parametric studies (not included in the main results for brevity) indicate that increasing the core thickness from 2 mm to 6 mm raises the overall damping ratio by approximately 35%, while a further increase to 8 mm yields only marginal gains (<5%) due to the core's near-incompressibility limiting additional shear deformation. The optimal core thickness of 4 mm (selected in Section 8.1) thus represents a trade-off where buckling load-to-weight ratio and damping performance are simultaneously near-maximum. This observation aligns with classical sandwich theory, which states that core shear flexibility dominates energy dissipation in the pre-buckling regime.

$$\varepsilon_r = \frac{\omega_{br} - \omega_{ar}}{2\omega_r} \quad (2)$$

In this study, we focus on a method that utilizes Frequency Response Function (FRF) curves obtained from hammer tests conducted on the specimens. Following the work of Alexander Presas et al. [37], the damping ratio is calculated by first identifying the peak corresponding to the natural frequency of the structure, as shown in the FRF diagram in Figure 12. Once the peak location is determined, the amplitude at this point A_{max} is recorded. Subsequently, the value of $\frac{A_{max}}{\sqrt{2}}$ is calculated, and a horizontal line at this level is drawn on the plot, intersecting the FRF curve at two points. The corresponding natural frequencies at these two points are then obtained, and the damping ratio of the structure is computed using the above relation for further discussion.

7. Numerical Simulation

The numerical simulation was performed using the finite element software ABAQUS. The geometric parameters are shown in Figure 4, and the Neo-Hookean strain energy density function was assigned to simulate the behavior of the hyperelastic core. The Neo-Hookean model was selected because the primary objective of the numerical analysis was the prediction of the critical buckling load, which occurs in the pre-buckling regime where global strains remain relatively small. Experimental observations indicated that buckling initiated before the core experienced large deformations associated with strong material nonlinearity. Therefore, the initial shear response provided by the Neo-Hookean formulation was considered sufficient for this purpose.

Neo-Hookean model justification:

Simplicity and Accuracy for Moderate Strains:

The neo-Hookean model provides a simple yet effective description of hyperelastic behavior for materials undergoing moderate strains, capturing the initial shear stiffness and volumetric response with only one material parameter. For the TPU core used in our specimens, pre-testing indicated that the material operates primarily in the moderate strain range during axial compression up to buckling.

Comparison with More Complex Models:

More complex hyperelastic models, such as Mooney-Rivlin or Ogden, include multiple material parameters and can more accurately capture highly nonlinear stress–strain behavior at large deformations. However, these models require extensive material characterization (multi-parameter curve fitting) and introduce additional computational complexity. In our case, the loading conditions and experimental observations showed that the neo-Hookean model captures the essential stiffness variation relevant to buckling prediction, without significantly compromising accuracy. This is also supported by the excellent agreement (≈3.6% discrepancy) between numerical predictions and experimental buckling loads.

Practical Considerations for Numerical Simulation:

Using a neo-Hookean model simplifies the finite-element implementation in ABAQUS, reduces convergence difficulties, and ensures computational efficiency while still providing reliable predictions of natural frequency evolution and critical buckling loads for the sandwich cylinders. Uniaxial tensile testing was used to calibrate the model to obtain the initial elastic properties governing structural stiffness. While buckling induces multiaxial stress states, the close agreement between experimental and numerical buckling loads (≈3.6% discrepancy) confirms that the chosen model adequately represents the material behavior within the scope of this study. The final model is illustrated in Figure 13, where the top and bottom edges of the shell are constrained, resulting in zero displacements and rotations at the shell edges. Overall, the applied boundary conditions in the FEM analysis are classified as clamped–clamped (C–C). After developing the model of the fabricated specimens, two separate analyses were conducted for VCT application. Following a convergence analysis, the optimal number of shell elements was determined to be 26,545. The initial step involves a buckling analysis to determine the critical buckling load (p_0). Subsequently, a free vibration analysis is performed to determine the first critical natural frequency (f_0). The convergence study evaluated four mesh densities: coarse (≈8,200 elements), medium (≈16,200 elements), fine (≈26,545 elements), and very fine (≈42,000 elements). The predicted buckling load changed by less than 0.8% between the fine and very fine meshes, and the natural frequency changed by less than 0.3%. Therefore, the fine mesh (26,545 shell elements for the face sheets and 124,000 solid elements for the core) was selected as providing mesh-independent results with reasonable computational cost (approximately 25 minutes per simulation on a workstation with 16 cores). The element aspect ratio was maintained below 5:1 in the core to avoid shear locking, and hourglass control was activated for the C3D8R elements. The S8R shell elements include transverse shear flexibility, which is essential because the sandwich construction has a non-negligible shear deformation contribution to the overall flexibility. This study in ABAQUS requires two solution steps:

1. The first step focuses on the free vibration of the structure (f_0) under the specified boundary conditions, particularly at the clamped ends, without applying any preload.
2. In the second step, the free vibration of the structure (f_l) is analyzed while applying a preload that varies from zero axial pressure (p_l) up to 70% of the numerical or analytical critical buckling load (p_0). This step enables the prediction of the actual critical buckling load using the first natural frequencies (f_l) measured under different preloads.

The interface between the hyperelastic TPU core and the composite face sheets was assumed to be perfectly bonded using a Tie constraint in ABAQUS. This assumption is justified by experimental observations, which showed no visible debonding or sliding at the interface up to the buckling load. However, we acknowledge that this simplification does not account for potential interfacial damage or delamination, which could become relevant in post-buckling or under cyclic loading conditions. The TPU hyperelastic core was meshed using 3D continuum solid elements (C3D8R – 8-node linear brick, reduced integration), while the inner and outer composite face sheets were modeled using S8R elements (8-node doubly curved thick shell, reduced integration). The two dissimilar meshes were connected by the aforementioned Tie constraint. Initially, all six degrees of freedom related to displacements and rotations are constrained, except for the axial displacement along the length on one side of the clamped boundary (see left side of Figure 13 where w≠0). This ensures that axial loading can be applied. It is crucial that this degree of freedom remains unconstrained, and the in-plane load applied at the edge is considered in the free vibration analysis. For an effective analysis of buckling and free vibration of the sandwich cylinder under axial in-plane loading applied at one side, a reference point is defined and connected to the entire upper edge. Additionally, a cap is used to ensure that the force is evenly distributed along the edge, aligning with laboratory conditions. The boundary conditions and overall model setup in ABAQUS are shown in Figure 13.

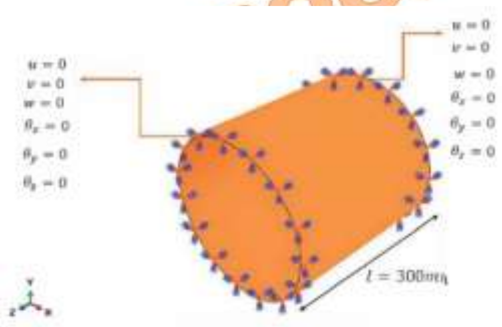

Fig. 13. Boundary conditions and loading setup

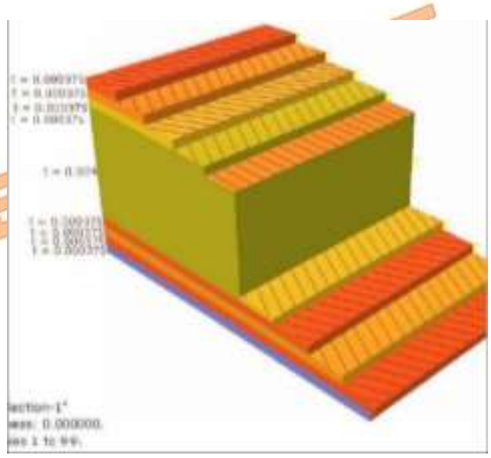

Fig. 14. Layer stacking configuration of the composite model

The layer stacking of the laminated composite model in ABAQUS is shown in Figure 14. The selected element type is S8R, which refers to a thick, two-sided shell element with 8-node curvature and reduced integration. The primary goal of the finite-element model is to predict global buckling behavior and natural frequency evolution of the sandwich cylinders. For relatively thin sandwich cores, the bending and axial stiffness of the core can be efficiently captured using shell elements, which significantly reduce computational cost and convergence issues compared with fully 3D continuum models. Previous studies on sandwich structures with compliant cores have shown that shell-based core modeling can reliably capture global deformation patterns and critical buckling loads, particularly when face sheets dominate bending stiffness.

Fig. 15. Mesh generated by the finite element software

Figure 15 illustrates the structural mesh of the model. Additionally, hyperelastic and composite materials were assigned to define the mechanical properties of the sandwich cylinder.

8. Results

8.1. Numerical Simulation Output

To achieve more accurate numerical results, a mesh convergence study and the identification of an optimal mesh size are essential. The results of the mesh convergence analysis for the buckling evaluation of the structure are shown in Figure 16. The total number of elements in the simulation is approximately 16,200, and the predicted buckling load shows excellent agreement with the experimental data, exhibiting a very small and acceptable error. It is noteworthy that increasing the number of elements beyond this point did not result in significant changes in the results, making this choice the most efficient in terms of computational time.

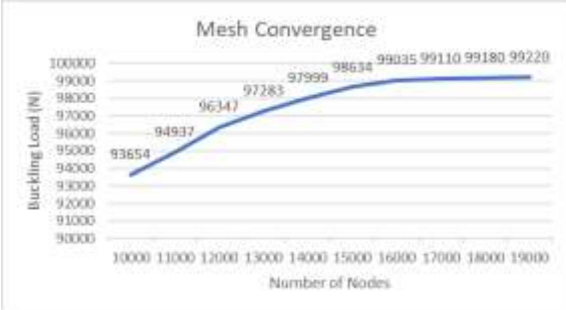

Fig. 16. Mesh convergence for the buckling load analysis

In Table 2, the mode shapes for the first to third buckling and vibration modes of the sandwich cylinder with optimal dimensions are presented. This section also includes a comparison of the knockdown factor values corresponding to the composite face sheets.

Table 2. Natural frequencies (Hz) and buckling loads (KN) for the first to third modes

No.	$f_0(Hz)$	$p_o\,(KN)$	Buckling modes	Vibration modes
1	255.37	99.035	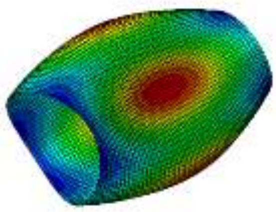	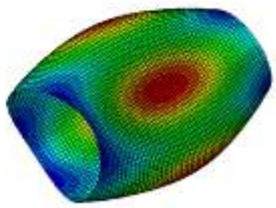
2	418.32	137.104	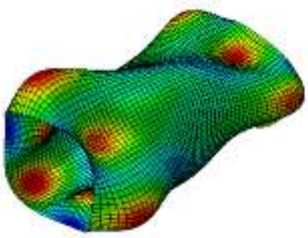	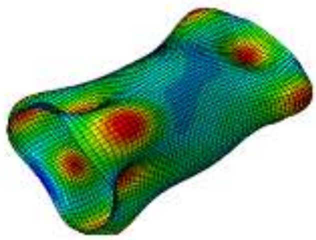

3	600.51	138.127	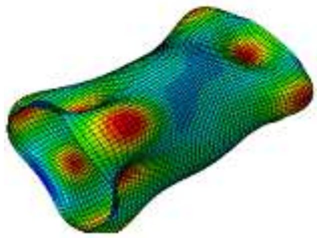	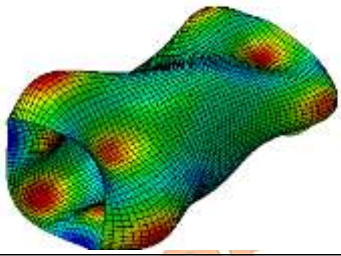

The numerical critical buckling load was obtained as 99.035 kN with a natural frequency of 255.37 Hz. Once the critical buckling load is determined from the numerical analysis, various percentages of this load — typically ranging from 10% to 70% of the critical buckling load — are applied to the structure. The resulting frequencies, used for VCT calculations, are presented in Table 3. The buckling load results obtained from the parametric study of the optimal core thickness and fiber orientation angles are presented in Table 4.

Table 3. Natural frequencies corresponding to different percentages of the critical buckling load

Percentage of $\boldsymbol{P_{cr}}$	Applied Load (KN)	Natural Frequency (Hz)
0.1 P_{cr}	9.903	246.37
0.2 P_{cr}	19.807	239.78
0.3 P_{cr}	29.710	229.76
0.4 P_{cr}	39.614	218.45
0.5 P_{cr}	49.517	207.94
0.6 P_{cr}	59.421	196.58
0.7 P_{cr}	69.324	185.79

UNCORRECTED PROOF
UNCORRECTED PROOF

Table 4. Effect of fiber orientation and core thickness variations on natural frequency and buckling load

PARAMETRIC STUDY OF OPTIMUM CORE THICKNESS AND LAYUP ANGLE OF FACES EACH FACE CONSISTS OF 4 LAYERS ITSELF THICKNESS OF INNER AND OUTER FACES=1.5 mm INSIDE DIAMETER=155 mm							
ROW	CORE THICKNESS(M)	LAY UP ANGLE (degrees)	WEIGHT (KG)	Critical load (N)	CRIT. LOAD/ WEIGHT	NATURAL FREQUENCY(HZ)	NAT.FREQ./ WEIGHT
1	1.00E-03	15/-15	0.926	38270.53	41328.87	217.08	234.42
2		30/-30	0.926	38882.64	41989.89	222.07	239.82
3		45/-45	0.926	35540.97	38381.18	206.86	223.39
4		52.5/-52.5	0.926	34033.36	36753.09	206.03	222.49
5		60/-60	0.926	33736.38	36432.37	203.80	220.09
6		67.5/-67.5	0.926	32262.78	34841.01	202.66	218.85
7		75/-75	0.926	32081.41	34645.15	202.07	218.22
8		0/90	0.926	28664.92	30955.64	198.39	214.24
9	2.00E-03	15/-15	1.19	55831.31	46917.07	238.74	200.62
10		30/-30	1.19	56724.54	47667.68	244.27	205.27
11		45/-45	1.19	51850.32	43571.70	227.54	191.21
12		52.5/-52.5	1.19	49905.17	41937.12	226.63	190.44
13		60/-60	1.19	49215.98	41357.97	224.17	188.38
14		67.5/-67.5	1.19	46069.28	38713.68	222.67	187.12
15		75/-75	1.19	46801.54	39329.03	222.28	186.79
16		0/90	1.19	38510.84	32362.05	218.22	183.38
17	3.00E-03	15/-15	1.45	74065.41	51079.59	250.79	172.96
18		30/-30	1.45	77316.40	53321.66	256.88	177.16
19		45/-45	1.45	71474.14	49292.51	252.22	173.95
20		52.5/-52.5	1.45	70274.86	48465.42	251.68	173.57
21		60/-60	1.45	68814.86	47458.52	249.72	172.22
22		67.5/-67.5	1.45	68010.05	46903.48	249.37	171.98
23		75/-75	1.45	67023.87	46223.36	248.10	171.10
24		0/90	1.45	57243.70	39478.41	237.97	164.12
25	4.00E-03	15/-15	1.71	87105.64	50938.97	245.44	143.53
26		30/-30	1.71	99035.00	57915.20	257.32	150.48
27		45/-45	1.71	84289.93	49292.36	252.22	147.50
28		52.5/-52.5	1.71	83618.88	48899.93	249.93	146.16
29		60/-60	1.71	81948.04	47922.83	248.95	145.59
30		67.5/-67.5	1.71	80059.56	46818.46	246.00	143.86
31		75/-75	1.71	77792.49	45492.68	244.94	143.24
32		0/90	1.71	70653.46	41317.81	239.51	140.06
33	5.00E-03	15/-15	1.97	102134.09	51844.72	237.28	120.45
34		30/-30	1.97	109898.83	55786.21	247.77	125.77
35		45/-45	1.97	101950.46	51751.50	245.52	124.63
36		52.5/-52.5	1.97	100030.25	50776.78	242.73	123.21
37		60/-60	1.97	98563.45	50032.21	239.61	121.63
38		67.5/-67.5	1.97	97248.54	49364.74	236.30	119.95
39		75/-75	1.97	95332.86	48392.32	232.60	118.07
40		0/90	1.97	86196.54	43754.59	221.38	112.38
41	6.00E-03	15/-15	2.23	112920.85	50637.15	232.12	104.09
42		30/-30	2.23	120733.20	54140.45	241.40	108.25
43		45/-45	2.23	110302.37	49462.95	235.37	105.55
44		52.5/-52.5	2.23	108842.38	48808.24	231.64	103.88
45		60/-60	2.23	108248.40	48541.88	227.85	102.18
46		67.5/-67.5	2.23	106314.58	47674.70	225.67	101.20
47		75/-75	2.23	103802.66	46548.28	223.36	100.16
48		0/90	2.23	95570.91	42856.91	217.62	97.59
49	1.50E-03	15/-15	1.056	46123.69	41146.61	215.00	227.04
50		30/-30	1.056	46861.40	41804.72	219.95	232.27
51		45/-45	1.056	42834.02	38211.92	204.88	216.36

52		52.5/-52.5	1.056	41017.05	36591.01	204.06	215.49
53		60/-60	1.056	40659.12	36271.70	201.85	213.16
54		67.5/-67.5	1.056	38883.13	34687.36	200.72	211.96
55		75/-75	1.056	38664.55	34492.37	200.14	211.35
56		0/90	1.056	34547.00	30819.13	196.50	207.50
57	2.50E-03	15/-15	1.32	64190.02	45810.77	185.15	244.40
58		30/-30	1.32	65216.98	46543.68	189.44	250.06
59		45/-45	1.32	59613.03	42544.28	176.47	232.94
60		52.5/-52.5	1.32	57376.66	40948.24	175.76	232.00
61		60/-60	1.32	56584.29	40382.75	173.85	229.49
62		67.5/-67.5	1.32	52966.48	37800.81	172.69	227.95
63		75/-75	1.32	53808.37	38401.65	172.38	227.55
64		0/90	1.32	44276.44	31598.96	169.24	223.39
65	3.50E-03	15/-15	1.58	79894.07	47635.57	156.25	246.87
66		30/-30	1.58	83400.90	49726.46	160.05	252.88
67		45/-45	1.58	77098.88	45968.98	157.14	248.29
68		52.5/-52.5	1.58	75805.21	45197.66	156.81	247.75
69		60/-60	1.58	74230.32	44258.65	155.59	245.83
70		67.5/-67.5	1.58	73362.17	43741.03	155.37	245.48
71		75/-75	1.58	72298.38	43106.77	154.58	244.23
72		0/90	1.58	61748.55	36816.60	148.26	234.26
73	4.50E-03	15/-15	1.84	93800.32	48024.23	130.88	240.82
74		30/-30	1.84	104379.46	53440.58	137.22	252.48
75		45/-45	1.84	90768.20	46471.84	134.50	247.47
76		52.5/-52.5	1.84	90045.57	46101.86	133.28	245.23
77		60/-60	1.84	88246.32	45180.68	132.76	244.27
78		67.5/-67.5	1.84	86212.70	44139.50	131.18	241.37
79		75/-75	1.84	83771.38	42889.58	130.61	240.33
80		0/90	1.84	76083.67	38953.60	127.72	235.00
81	5.50E-03	15/-15	2.1	108035.30	48464.12	111.60	234.37
82		30/-30	2.1	116248.67	52148.60	116.54	244.73
83		45/-45	2.1	107841.05	48376.98	115.48	242.51
84		52.5/-52.5	2.1	105809.89	47465.81	114.17	239.75
85		60/-60	2.1	104258.34	46769.79	112.70	236.67
86		67.5/-67.5	2.1	102867.46	46145.85	111.14	233.40
87		75/-75	2.1	100841.10	45236.83	109.40	229.74
88		0/90	2.1	91176.89	40901.52	104.13	218.67
89	6.50E-03	15/-15	2.36	116151.43	46364.60	95.54	225.48
90		30/-30	2.36	124187.29	49572.30	99.36	234.50
91		45/-45	2.36	113458.05	45289.47	96.88	228.64
92		52.5/-52.5	2.36	111956.28	44690.00	95.35	225.02
93		60/-60	2.36	111345.31	44446.12	93.79	221.34
94		67.5/-67.5	2.36	109356.17	43652.11	92.89	219.22
95		75/-75	2.36	106772.38	42620.73	91.94	216.97
96		0/90	2.36	98305.12	39240.82	89.57	211.39
				124187.29	53440.58	219.95	252.88

To minimize material usage and time prior to the experimental and fabrication stages, the above table was obtained through a parametric study, performing various analyses to identify the optimal parameters. This section focuses on determining the ideal fiber orientation angles for the composite face sheets along with the core thickness, by evaluating the buckling load in different configurations. As shown in Figures 17 and 18, various values of core thickness and fiber orientation angles are considered to achieve the best results.

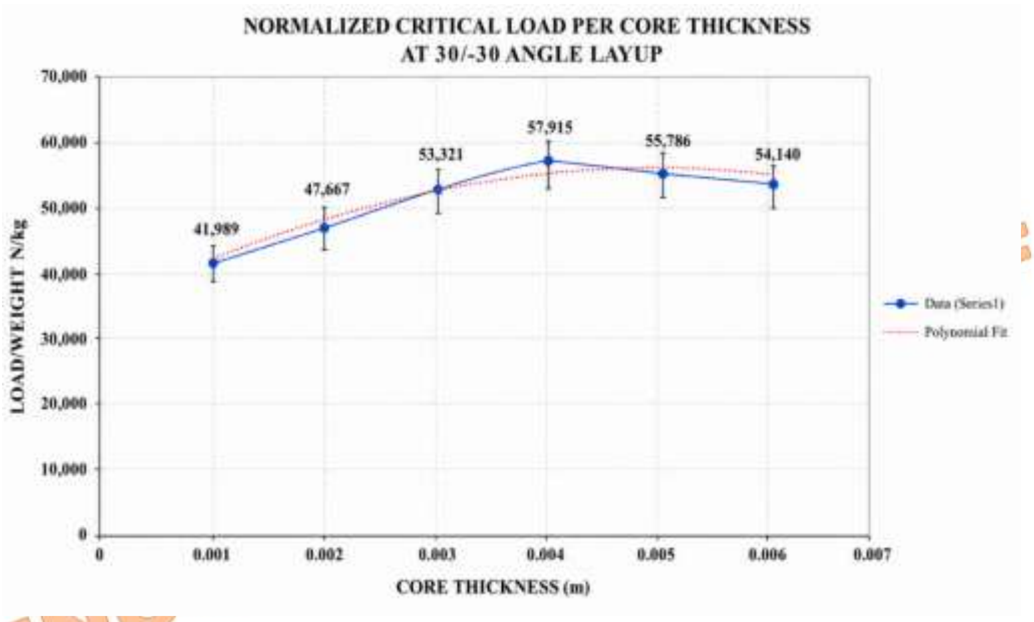

Figure 17. Buckling load as a function of core thickness

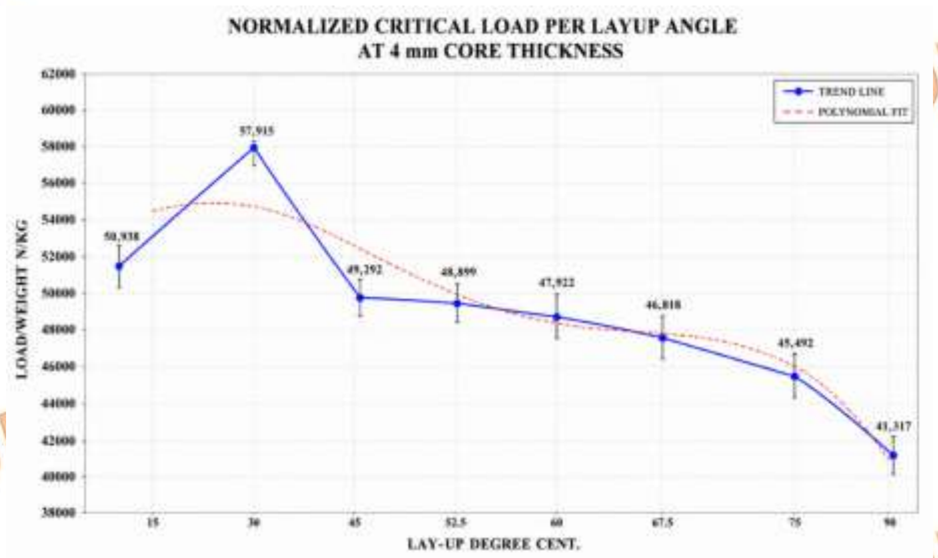

Figure 18. Buckling load as a function of fiber stacking angle

The data presented in the graphs clearly indicate that increasing the core thickness leads to a higher buckling load. However, when this parameter is evaluated in relation to the structural weight ratio, a core thickness of 4 mm emerges as the optimal value. Once the core thickness was finalized, the next step was to determine the ideal fiber orientation angle for this thickness based on the numerical outputs. It was found that an angle of 0/90° corresponds to the minimum buckling load for the structure. In this scenario, the buckling load reached its lowest value among the angles analyzed. In contrast, the ±30° configuration produced the maximum buckling load. It is important to note that as the fiber winding angle increases, the fibers begin to orient perpendicular to the cylinder rather than remaining axial (parallel to the radial direction). This change negatively affects the axial buckling resistance of the structure. Essentially, when the fibers are aligned parallel to the cylinder's radial direction, they become less effective in resisting axial buckling, an effect highlighted in this numerical study. While the Neo-Hookean model proved adequate for buckling load prediction (error ≈ 3.6% after VCT), it is important to acknowledge its limitations for larger strain analyses. The TPU material exhibits moderate strain-softening beyond 25% strain (visible in Figure 19), which the Neo-Hookean model cannot capture because it assumes a constant shear modulus. For future studies involving post-buckling behavior or large deformation (>30% strain), more sophisticated hyperelastic models such as Mooney-Rivlin (two parameters) or Ogden (third-order) are recommended.

Additionally, the current model neglects strain-rate sensitivity and hysteresis, which are known characteristics of TPU but were assumed negligible under the quasi-static loading conditions applied here (axial displacement rate of 0.5 mm/min). Researchers aiming to simulate dynamic buckling or impact scenarios should incorporate viscoelastic material models, such as a Prony series, into the ABAQUS material definition. These extensions are beyond the scope of the present work but represent valuable directions for future research.

8.2. Tensile Test Results

Figure 19 shows the force-displacement curve obtained from the output of the universal tensile testing machine.

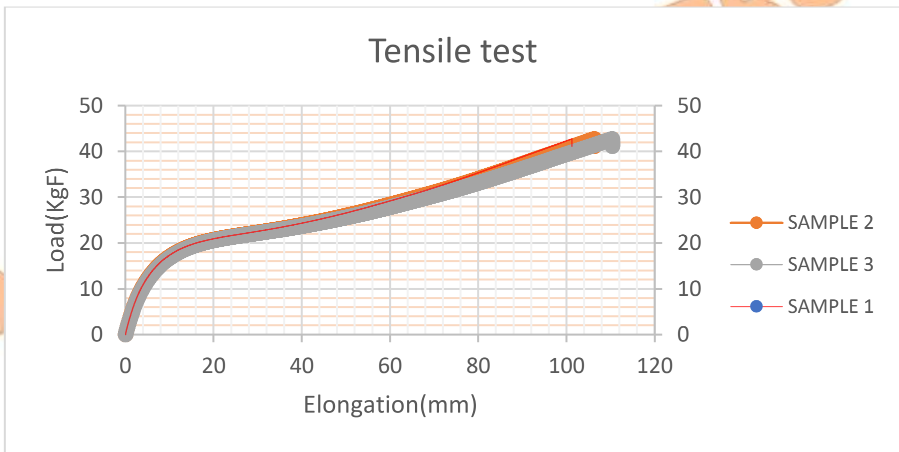

Fig. 19. Force–displacement curve of the tensile test specimens

The mechanical properties of the materials are presented in Table 5. The Neo-Hookean parameter C_{10} = 0.65 MPa (reported in Table 5) was derived from the initial linear portion of the uniaxial tensile stress-strain curve (Figure 19). For a nearly incompressible hyperelastic material, the initial Young's modulus E is related to C_{10} by $E = 2C_{10}(1+\nu)$. Using the experimentally measured E ≈ 1.81 MPa and ν = 0.39, we obtained C_{10} = 0.65 MPa. This parameter captures the small-to-moderate strain stiffness relevant to pre-buckling deformation.

Table 5: Mechanical properties

Parameter	TPU	Composite layer
$\boldsymbol{E_1} = \boldsymbol{E_2}$ (MPa)	-	1250
$\boldsymbol{E_3}$ (MPa)	-	811
Poisson's ratio $\boldsymbol{\nu}$	0.39	-
Density $\boldsymbol{\rho}$ $(\boldsymbol{kg/m^3})$	1220	1973
$\boldsymbol{G_{12}} = \boldsymbol{G_{13}}$ (GPa)	-	145
$\boldsymbol{G_{23}}$ (MPa)	-	178
$\boldsymbol{C_{10}}$ (MPa)	0.65	-
$\boldsymbol{\nu_{12}} = \boldsymbol{\nu_{13}}$	-	0.28
Melting Temperature °C	210	-

Using the method described, the damping coefficients of the specimens containing composite layers can be determined from the FRF (Frequency Response Function) diagrams of the experimental samples, some of which are illustrated in Figure 20.

The experimental tensile stress-strain curve (average of three specimens) with the Neo-Hookean model prediction using the derived C_{10} = 0.65 MPa and ν = 0.39. The model captures the initial stiffness very well and remains within 8% of the experimental stress up to a strain of 20%, which covers the pre-buckling deformation range observed in our compression tests (maximum axial strain < 12%). This confirms that the Neo-Hookean model is adequate for the buckling load prediction in this study.

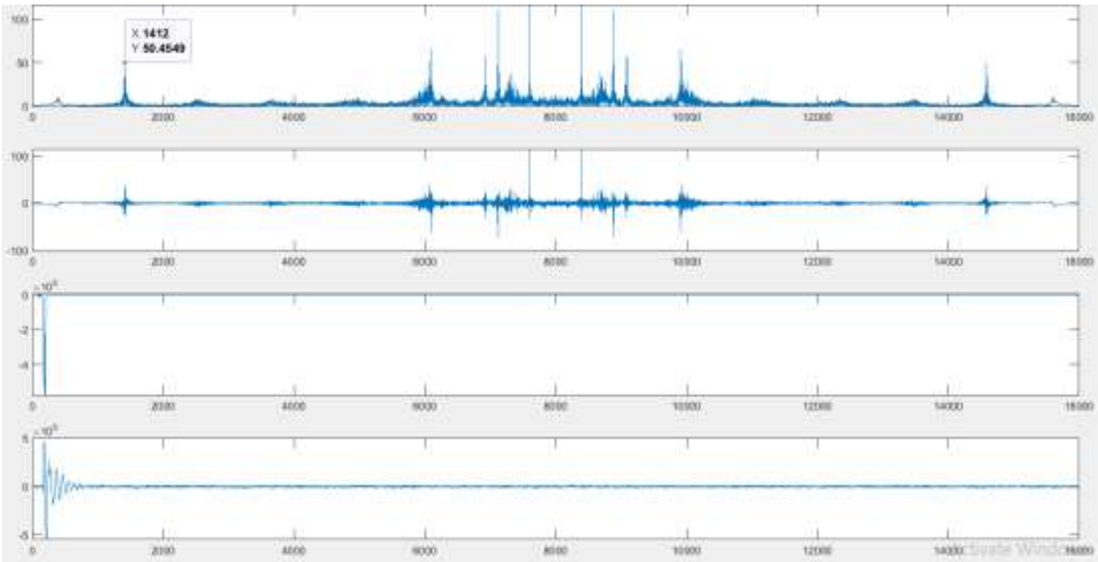

Fig. 20. Frequency Response Function (FRF)

Furthermore, a review of previous studies indicates that this method is repeatable and demonstrates satisfactory correlation under various scenarios, exhibiting a relatively small margin of error.

The loading curve up to the buckling stage is presented in Figure 21. The actual data points and outputs recorded by the testing machine show negative values in the vertical force column, which is due to the compressive nature of the applied load during the buckling test.

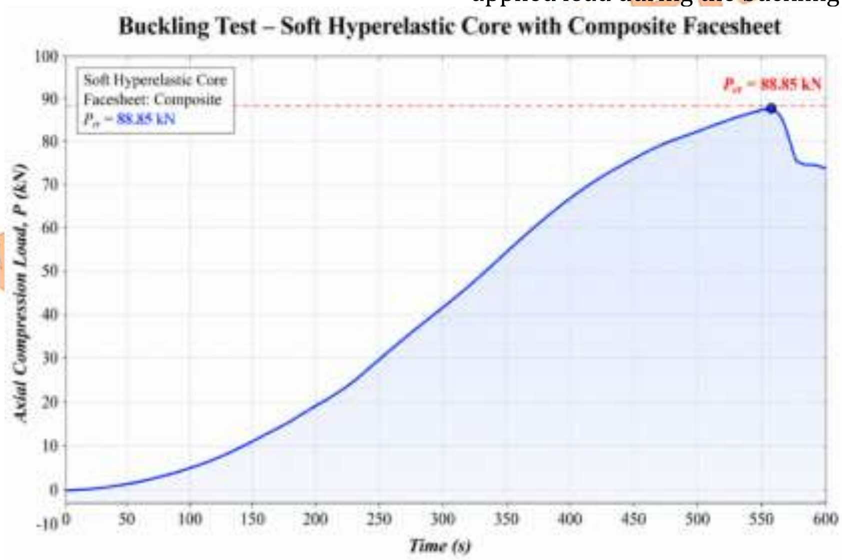

Fig. 21. Buckling diagram of the cylinder

8.3 Damping Coefficient Results

As previously mentioned, the damping coefficient remains nearly constant for any given structure. The damping coefficients for three different configurations of cylindrical shells are presented in Table 7 to evaluate the effects of adding a hyperelastic core and converting the structure from a single-layer composite into a sandwich configuration. The first configuration (A) represents a single-layer composite shell, the second (B) consists of inner and outer composite layers, and the third (C) includes a hyperelastic core with inner and outer composite layers. All three configurations have identical inner and outer diameters, heights, and thicknesses, meaning that all geometrical parameters are consistent across the samples for valid comparison. The only difference lies in their structural composition: the first is a single-layer composite cylinder, the second is a sandwich-type shell composed of two layers without a core, and the third is the main structure discussed in this study — a sandwich structure with a soft (hyperelastic) core. According to the calculations presented in Table 6, the damping coefficient for the cylinder with composite layers and a soft core is determined to be 0.64%. The indices b and a correspond to the points with higher and lower frequencies relative to the natural frequency, respectively (as shown in Figure 12).

Table 6. Damping coefficient calculations

<table>
<tr><td>A</td><td colspan="4">Single layer composite shell</td><td>0.37</td></tr>
<tr><td>B</td><td colspan="4">Sandwich shell with inner and outer composite layers</td><td>0.42</td></tr>
<tr><td rowspan="5">C
Sandwich shell with soft core and composite faces</td><td rowspan="2">Amplitude</td><td>A_a</td><td>A_{max}</td><td>A_b</td><td rowspan="5">0.64</td></tr>
<tr><td>35.67</td><td>50.45</td><td>65.31</td></tr>
<tr><td rowspan="3">Frequency (Hz)</td><td>F_a</td><td>F_{max}</td><td>F_b</td></tr>
<tr><td>1405.00</td><td>1412.00</td><td>1421.00</td></tr>
<tr><td>232.72</td><td>224.84</td><td>226.62</td></tr>
</table>

It is worth noting that for vibrating structures, a damping ratio of approximately 0.7% is considered optimal. In this study, the composite structure that was fabricated and tested achieved a damping ratio of 0.64%. A comparison of the damping ratios among the three structural configurations shows a slight increase from Type A to Type B, which can be attributed to the greater degrees of freedom in the sandwich structure. This occurs because a monolithic structure is divided into multiple layers, introducing additional parameters and mechanisms for vibration dissipation. This indicates an acceptable level of damping performance for the structure. Finally, comparing Type B with Type C reveals a significant improvement, which highlights the beneficial effects of the added soft core. When these damping characteristics are combined with the structure's buckling properties, they provide an ideal balance, allowing the structure to effectively resist both buckling forces and vibrational damping simultaneously.

8.4 Results of the Vibration Correlation Technique (VCT)

To compare the numerical and analytical results with the actual experimental data, a destructive buckling test was conducted on the specimen. Accordingly, the cylinder with composite surfaces and a hyperelastic core buckled under a load of 88,853.7 N. As discussed in previous sections, the critical buckling load can be determined using analytical and numerical methods. Subsequently, various portions of the buckling load and their corresponding frequencies at each stage are calculated. Based on the following diagram, the computations are applied using the Vibration Correlation Technique (VCT) to estimate the actual buckling load. The detailed results and the parameters used in the VCT experiments for the composite layers of the cylindrical shell are presented in Table 7. The restraint coefficient (ξ^2) is determined using a second-order curve-fitting diagram of $(1-P)^2$ versus $1-f^2$, as described in the previous section and illustrated in Figure 23.

Table 7. Summary of VCT calculation results, buckling load (KN) and natural frequency (Hz)

ROW	Pcr [KN] buckling	99.04	Natural frequency [HZ]	255.37	Section ROW
1	0.10*Pcr	9.90	frequency for 0.10*Pcr	246.37	1
2	0.20*Pcr	19.81	frequency for 0.20*Pcr	239.78	2
3	0.30*Pcr	29.71	frequency for 0.30*Pcr	229.76	3
4	0.40*Pcr	39.61	frequency for 0.40*Pcr	218.45	4
5	0.50*Pcr	49.52	frequency for 0.50*Pcr	207.94	5
6	0.60*Pcr	59.42	frequency for 0.60*Pcr	196.58	6
7	0.70*Pcr	69.32	frequency for 0.70*Pcr	185.79	7
8	normalized loads P	0.1	normalized frequencies F	0.96	1
9		0.2		0.94	2
10		0.3		0.90	3
11		0.4		0.86	4
12		0.5		0.81	5
13		0.6		0.77	6
14		0.7		0.73	7
15	1-P	0.9	F^2	0.93	1
16		0.8		0.88	2
17		0.7		0.81	3
18		0.6		0.73	4
19		0.5		0.66	5
20		0.4		0.59	6
21		0.3		0.53	7
22	(1-P) ^2	0.81	1-F^2	0.07	1
23		0.64		0.12	2
24		0.49		0.19	3
25		0.36		0.27	4
26		0.25		0.34	5
27		0.16		0.41	6
28		0.09		0.47	7

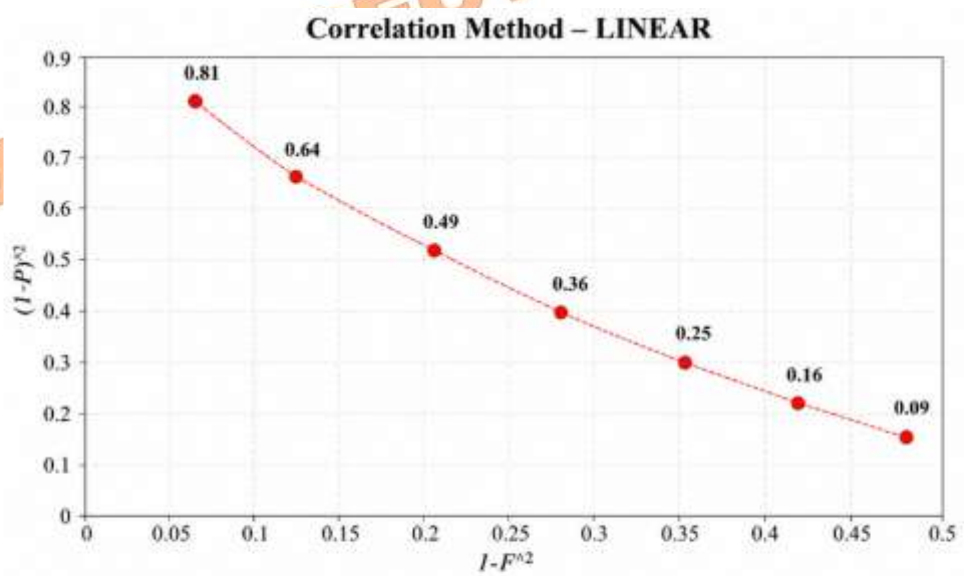

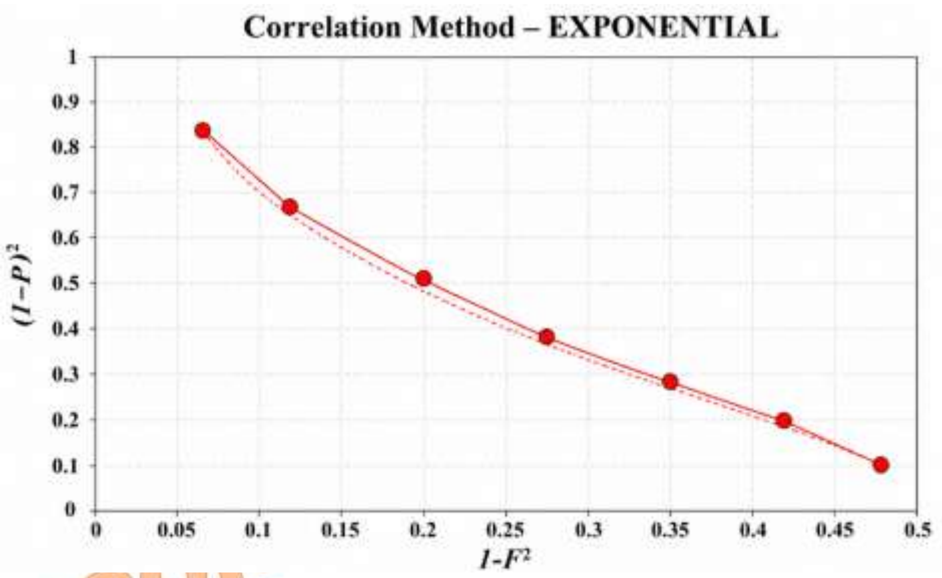

Fig. 22. Curve fitting of the Vibration Correlation Technique (VCT) plots

The failure coefficient is calculated from the plot in Figure 23 as ξ^2 = 0.05. Accordingly, the experimental critical buckling load is determined as:

$$P_{Critical-Experimental} = P_{Numerical}\left(1-\sqrt{\xi^2}\right) \quad (3)$$

$$= P_{cr} * 0.95 = 0.95 * 99.03 = 94.469 \text{ KN}$$

In Table 8, the buckling results obtained from the experimental method, VCT, and ABAQUS are compared.

Table 8. Comparison of buckling loads (N) obtained from different methods

Method	Buckling Load (N)	Error (%)	Specimen Configuration
Experimental	88,854	—	Composite faces + TPU core
VCT	94,469	6.32	Composite faces + TPU core
FEM (ABAQUS)	99,035	11.46	Composite faces + TPU core

Table 8 compares the experimentally measured buckling load with predictions from the Vibration Correlation Technique (VCT) and finite element modeling (FEM). The destructive test yielded a critical load of 88,853.7 N, which serves as the reference value. The VCT prediction shows closer agreement with the experimental result than the FEM prediction, which differs by approximately 3.6%. This improved accuracy arises from the inherent capability of VCT to account for structural imperfections by effectively combining experimental and numerical information. In contrast, FEM results are influenced by idealized boundary conditions and material assumptions. In principle, VCT predictions yield values slightly lower than purely numerical results, reflecting the realistic behavior of imperfect structures. Overall, the strong correlation among experimental, VCT, and numerical results confirms the reliability of VCT as a practical and cost-effective method for predicting buckling loads in sandwich structures with a hyperelastic core.

9. Conclusions

Cylindrical sandwich structures with composite face sheets and hyperelastic cores represent a promising solution for applications requiring high buckling resistance combined with effective vibration damping. The present study demonstrated that incorporating a soft hyperelastic core significantly enhances the dynamic performance of the structure, while the composite faces maintain their load-carrying capability. In particular, an improvement of approximately 72% in damping ratio was observed for cylinders with identical geometric parameters when a hyperelastic core was introduced, highlighting the effectiveness of this design concept for vibration mitigation and fatigue reduction in practical engineering applications.

From a stability assessment perspective, the Vibration Correlation Technique (VCT) proved to be a reliable non-destructive method for estimating the critical buckling load of sandwich cylinders with hyperelastic cores. The experimental results showed that VCT predictions were in closer agreement with measured buckling loads than those obtained from the finite element model, achieving an approximate 45% reduction in error relative to the numerical predictions. This outcome indicates that VCT is not only effective in avoiding destructive testing but also less sensitive to certain modeling assumptions inherent in numerical simulations. It should be noted, however, that the finite element analysis employed a simplified Neo-Hookean constitutive model to represent the hyperelastic behavior of the TPU core. While this model captures the primary nonlinear elastic response, it does not fully account for strain-rate effects, material hysteresis, or large-strain nonlinearities that are characteristic of real hyperelastic polymers. This simplification likely contributed to the observed discrepancies between numerical and experimental buckling loads and represents a key limitation of the present numerical framework.

Beyond validating VCT for buckling load prediction, the findings suggest broader implications for the design of lightweight cylindrical structures in aerospace, marine, and civil engineering systems, where simultaneous requirements for stability and vibration control are critical. The combination of composite face sheets and hyperelastic cores offers a viable pathway toward structures with enhanced service life and reduced maintenance demands.

Future work should focus on improving the numerical accuracy by adopting more advanced constitutive models for the hyperelastic core, such as Mooney–Rivlin or Ogden formulations, and by incorporating viscoelastic effects and geometric imperfections. Additionally, extending the experimental program to different core materials, loading paths, and environmental conditions would further clarify the applicability and robustness of VCT for complex sandwich structures.

Nomenclature

All variables used in this work are listed in the nomenclature.

θ	Fiber orientations relative to the horizontal axis
t	Core thickness
h	Thickness of each layer
R	Inner diameter of the cylinder
L	Overall cylinder length
P_0	Critical buckling load
f_0	Natural frequency
ξ^2	Knockdown factor

Conflicts of Interest

The authors declare that there is no conflict of interest regarding the publication of this article.

Appendixes

Appendixes appear after Conflicts of Interest.

References

[1] Arbelo, M.A., De Almeida, S.F., Donadon, M.V., Rett, S.R., Degenhardt, R. and Castro, S.G., 2014. Vibration correlation technique for the estimation of real boundary conditions and buckling load of unstiffened plates and cylindrical shells. Thin-Walled Structures, 79, pp.119–128. doi: 10.1016/j.tws.2014.01.012

[2] Kalnins, K., Arbelo, M.A., Ozolins, O., Skukis, E., Castro, S.G. and Degenhardt, R., 2015. Experimental nondestructive test for estimation of buckling load on unstiffened cylindrical shells using vibration correlation technique. Shock and Vibration, 2015, p.729684. doi: 10.1155/2015/729684

[3] Abramovich, H., Govich, D. and Grunwald, A., 2015. Buckling prediction of panels using the vibration correlation technique. Progress in Aerospace Sciences, 78, pp.62–73. doi: 10.1016/j.paerosci.2015.07.003

[4] Pagani, A. and Carrera, E., 2023. Unified one-dimensional finite element for the analysis of hyperelastic soft materials and structures. Mechanics of Advanced Materials and Structures, 30(2), pp.342–355. doi: 10.1080/15376494.2021.2013585

[5] Aranda-Iglesias, D., Rodríguez-Martínez, J.A. and Rubin, M.B., 2018. Nonlinear axisymmetric vibrations of a hyperelastic orthotropic cylinder. International Journal of Non-Linear Mechanics, 99, pp.131–143. doi: 10.1016/j.ijnonlinmec.2017.12.005

[6] Zhang, J., Xu, J., Yuan, X., Zhang, W. and Niu, D., 2019. Strongly nonlinear vibrations of a hyperelastic thin-walled cylindrical shell based on the modified Lindstedt–Poincaré method. International Journal of Structural Stability and Dynamics, 19(12), p.1950160. doi: 10.1142/S021945541950160X

[7] Wagner, H.N.R., Köke, H., Dähne, S., Niemann, S., Hühne, C. and Khakimova, R., 2019. Decision tree-based machine learning to optimize the laminate stacking of composite cylinders for maximum buckling load and minimum imperfection sensitivity. Composite Structures, 220, pp.45–63. doi: 10.1016/j.compstruct.2019.03.078

[8] Pitton, S.F., Ricci, S. and Bisagni, C., 2019. Buckling optimization of variable stiffness cylindrical shells through artificial intelligence techniques. Composite Structures, 230, p.111513. doi: 10.1016/j.compstruct.2019.111513

[9] Franzoni, F., Odermann, F., Lanbans, E., Bisagni, C., Arbelo, M.A. and Degenhardt, R., 2019. Experimental validation of the vibration correlation technique robustness to predict buckling of unstiffened composite cylindrical shells. Composite Structures, 224, p.111107. doi: 10.1016/j.compstruct.2019.111107

[10] Mohammadzadeh Gheshlaghi, R. and Ghaffarzadeh, S., 2025. Construction of a four-degree-of-freedom filament winding machine for production of composite lattice structures. Iranian Journal of Manufacturing Engineering. [In Persian]

[11] Höller, R., Libisch, F. and Hellmich, C., 2022. A membrane theory for circular graphene sheets, based on a hyperelastic material model for large deformations. Mechanics of Advanced Materials and Structures, 29(15), pp.2145–2160. doi: 10.1080/15376494.2020.1785598

[12] Xu, J., Yuan, X., Zhang, H., Zheng, F. and Chen, L., 2020. Nonlinear vibrations of thermo-hyperelastic moderately thick cylindrical shells with 2:1 internal resonance. International Journal of Structural Stability and Dynamics, 20(05), p.2050067. doi: 10.1142/S0219455420500673

[13] Khaniki, H.B., Ghayesh, M.H., Chin, R. and Amabili, M., 2021. Large amplitude vibrations of imperfect porous-hyperelastic beams via a modified strain energy. Journal of Sound and Vibration, 513, p.116416. doi: 10.1016/j.jsv.2021.116416

[14] Aurilia, M., Piscitelli, F., Sorrentino, L., Lavorgna, M. and Iannace, S., 2011. Detailed analysis of dynamic mechanical properties of TPU nanocomposite: The role of the interfaces. European Polymer Journal, 47, pp.925–936. doi: 10.1016/j.eurpolymj.2011.01.005

[15] Mehta, S., Raju, G., Kumar, S. and Saxena, P., 2022. Instabilities in a compressible hyperelastic cylindrical channel under internal pressure and external constraints. International Journal of Non-Linear Mechanics, 144, p.104031. doi: 10.1016/j.ijnonlinmec.2022.104031

[16] Saeidiha, M., Ahmadi, H. and Jalali, A., 2023. Nonlinear vibrations analysis of hyperelastic cylindrical shells utilizing the method of multiple scales. International Journal of Structural Stability and Dynamics, 23(05), p.2350095. doi: 10.1142/S0219455423500954

[17] Duc, N.D., Foroutan, K., Varedi-Koulaei, S.M. and Ahmadi, H., 2024. Nonlinear vibration analysis of laminated composite cylindrical shell under external loading utilizing meta-heuristic optimization algorithms. Iranian Journal of Science and Technology – Transactions of Mechanical Engineering, 48(2), pp.757–777. doi: 10.1007/s40997-023-00676-4

[18] Coskun, O. and Turkmen, H.S., 2023. Pre-trained design optimization of variable stiffness composite cylinders modeled using Bézier curves. Structural and Multidisciplinary Optimization, 66(2), p.41. doi: 10.1007/s00158-022-03485-6

[19] Zhang, J., Zhang, W. and Zhang, Y.F., 2023. Nonlinear resonant responses of hyperelastic cylindrical shells with initial geometric imperfections. Chaos, Solitons & Fractals, 173, p.113709. doi: 10.1016/j.chaos.2023.113709

[20] Pagani, A., Chiaia, P., Filippi, M. and Cinefra, M., 2024. Unified three-dimensional finite elements for large strain analysis of compressible and nearly incompressible solids. Mechanics of Advanced Materials and Structures, 31(1), pp.117–137. doi: 10.1080/15376494.2023.2229832

[21] Choudhary, P.K., 2023. Optimal design of composite cylindrical shells subject to compression buckling strength. Multidisciplinary Modeling in Materials and Structures, 19(5), pp.829–847. doi: 10.1108/MMMS-02-2023-0042

[22] Xin, R., Le, V.T. and Goo, N.S., 2024. Prediction of the buckling mode of cylindrical composite shells with imperfections using a FEM-based deep learning approach. Advanced Composite Materials, 33(2), pp.189–211. doi: 10.1080/09243046.2023.2206789

[23] Arani, M.S., Bakhtiari, M., Toorani, M. and Lakis, A.A., 2024. Studying the nonlinear response of incompressible hyperelastic thin circular cylindrical shells with geometric imperfections. Journal of the Mechanical Behavior of Biomedical Materials, 155, p.106562. doi: 10.1016/j.jmbbm.2024.106562

[24] Rezayat, H., Toozandehjani, H. and Zakeri, A., 2023. Experimental investigation of energy absorption in sandwich panels with composite/elastomer face sheets. Iranian Journal of Manufacturing Engineering. [In Persian]

[25] Liang, Z., Zhao, Y., Yu, H., Habibi, M. and Mahmoudi, T., 2024. Artificial neural networks coupled with numerical approach for the stability prediction of non-uniform functionally graded microscale cylindrical structures. Structures, 60, p.105826. doi: 10.1016/j.istruc.2023.105826

[26] Sobotka, Z., Horný, L., Chlup, H., Kohan, M., Hudák, R. and Valášek, M., 2025. Nonlinearly elastic and anisotropic constitutive model for EPTFE vascular graft based on tensile and inflation experiments. Mechanics of Advanced Materials and Structures, 32(3), pp.345–360. doi: 10.1080/15376494.2024.2448776

[27] Liu, F., Chen, H., Yang, J. and Wang, X., 2024. Application of physics-informed machine learning methods in buckling design of axially compressed cylindrical shells. Thin-Walled Structures, 200, p.111963. doi: 10.1016/j.tws.2023.111963

[28] Gao, P., Yu, T., Zhang, Y., Wang, J. and Zhai, J., 2021. Vibration analysis and control technologies of hydraulic pipeline system in aircraft: A review. Chinese Journal of Aeronautics, 34(4), pp.83–114. doi: 10.1016/j.cja.2020.07.013

[29] Bi, K. and Hao, H., 2016. Using pipe-in-pipe systems for subsea pipeline vibration control. Engineering Structures, 109, pp.75–84. doi: 10.1016/j.engstruct.2015.11.009

[30] Baciu, T.D., Degenhardt, R., Franzoni, F., Gliszczyński, A., Arbelo, M., Castro, S. and Kalnins, K., 2025. Vibration Correlation Technique for Predicting the Compressive Buckling Load of Cylindrical Shells under Combined Loading. Thin-Walled Structures, 216, p.113576. doi: 10.1016/j.tws.2025.113576

[31] Gliszczyński, A., 2025. VCT Based Buckling Load Prediction in Unstiffened CFRP Shells. Composite Structures, in press. doi: 10.1016/j.compositesb.2025.113201

[32] Yılmaz, H., 2025. Buckling of Steel Plates Under Rotational Restraints: Integration of Experimental Testing and the Vibration Correlation Technique. Experimental Mechanics, 65, pp.869–884. doi: 10.1007/s11340-025-01175-0

[33] Rahmani Gheshlaghi, M., Rahimi, G. and Hosseini, S., 2025. A Hybrid Computational Experimental Approach for Buckling Load Prediction in Hyperelastic Sandwich Shells Using the Vibration Correlation Technique. International Journal of Structural Stability and Dynamics, p.2650419. doi: 10.1142/S0219455426504195

[34] Souza, M.A., Fok, W.C. and Walker, A.C., 1983. Review of experimental techniques for thin-walled structures liable to buckling: Part I—Neutral and unstable buckling. Experimental Techniques, 7, pp.21–25. doi: 10.1111/j.1747-1567.1983.tb02115.x

[35] Breslavsky, I.D., Amabili, M. and Legrand, M., 2014. Nonlinear vibrations of thin hyperelastic plates. Journal of Sound and Vibration, 333(19), pp.4668–4681. doi: 10.1016/j.jsv.2014.05.008

[36] Breslavsky, I.D., Amabili, M. and Legrand, M., 2014. Physically and geometrically nonlinear vibrations of thin rectangular plates. International Journal of Non-Linear Mechanics, 58, pp.30–40. doi: 10.1016/j.ijnonlinmec.2013.09.002

[37] Presas, A., Valentin, D., Egusquiza, E., Valero, C., Egusquiza, M. and Bossio, M., 2017. Accurate determination of the frequency response function of submerged and confined structures using PZT-patches. Sensors, 17(3), p.660. doi: 10.3390/s17030660